Impact of dialcohol cellulose modification on the structural morphology and swelling behaviour of cellulose fibres

Citation for the original published paper (version of record):
Venkatraman, N., Jonasson, K., Lo Re, G. et al (2025). Impact of dialcohol cellulose modification on the structural morphology and swelling behaviour
of cellulose fibres. Cellulose, 32(14): 8101-8117. http://dx.doi.org/10.1007/s10570-025-06729-y

Cellulose (2025) 32:8101–8117
https://doi.org/10.1007/s10570-025-06729-y

ORIGINAL RESEARCH

Impact of dialcohol cellulose modification on the structural morphology and swelling behaviour of cellulose fibres

Nivedhitha Venkatraman · Katarina Jonasson · Giada Lo Re · Per A. Larsson · Anette Larsson

Received: 9 June 2025 / Accepted: 4 August 2025 / Published online: 23 August 2025

Abstract This study investigates how partial modification of softwood Kraft fibres into dialcohol cellulose affects fibre wall integrity and swelling behaviour across a modification range of ~25–~50%. Structural transformations within the fibre wall and the roles of the secondary cell wall layers in generating balloon-like morphologies during heterogeneous swelling were examined. A combination of optical microscopy techniques including polarised light, differential interference contrast and confocal laser scanning microscopy with dual fluorescent labelling was employed to visualise morphological changes. Results show that swelling intensified with increasing modification. At 51% modification, fibres exhibited uniform swelling, and the characteristic balloon-collar-like structures disappeared. Mild ballooning was observed in "never-dried" fibres with ~25% modification. Fibre width increased with modification, ranging from 35 ± 9 µm (unmodified) to 58 ± 24 µm (~50% modification), with greater variability at higher modification levels. Water retention values also rose, from 1.7 to 6.3 g water per gram of fibre. Finally, the modification-induced swelling introduced inelastic strain in the fibre wall, preserving balloon–collar morphology in air-dried fibres.

Keywords Dialcohol Cellulose · Balloon-Collar Morphology · Fibre Wall Swelling · Softwood Kraft Fibres and Confocal Microscopy

Supplementary Information The online version contains supplementary material available at https://doi.org/10.1007/s10570-025-06729-y.

N. Venkatraman · K. Jonasson · A. Larsson (✉)
Department of Chemistry and Chemical Engineering, Chalmers University of Technology, SE-412 96 Gothenburg, Sweden
e-mail: Anette.Larsson@Chalmers.se

N. Venkatraman · G. Lo Re · P. A. Larsson · A. Larsson
FibRe Centre for Lignocellulose-Based Thermoplastics, Chalmers University of Technology, SE-412 96 Gothenburg, Sweden

K. Jonasson
Tetra Pak Packaging Solutions AB, SE-221 86 Lund, Sweden

G. Lo Re
Department of Industrial Materials Science, Chalmers University of Technology, SE-412 96 Gothenburg, Sweden

G. Lo Re · A. Larsson
Wallenberg Wood Science Center, Chalmers University of Technology, SE-412 96 Gothenburg, Sweden

P. A. Larsson
Department of Fibre and Polymer Technology, KTH Royal Institute of Technology, SE-100 44 Stockholm, Sweden

Introduction

Cellulose is a readily available and abundant biodegradable polymer, a resource of significant current interest to both the forestry industry and our wider society. The development of innovative bio-based alternatives to replace conventional non-renewable packaging and barrier materials is necessary. Cellulose offers several advantages, notably its high mechanical strength and low oxygen permeability, positioning it as a promising sustainable alternative to synthetic thermoplastics (Hasan et al. 2021; Verma et al. 2024). However, native cellulose possesses a high glass transition temperature and degrades upon heating before it significantly softens or melts. Thus, it cannot be melted and processed to form complex shapes by traditional means, limiting its potential. Partial modification of cellulose fibres, achieved by converting cellulose into dialcohol cellulose (DALC), allows enhanced ductility while also introducing hygroscopic and thermoplastic properties (Larsson et al. 2013, 2014; Larsson & Wågberg 2016), which enabled its melt processing (Lo Re et al. 2023). The DALC fibres are obtained by a two-step process, where the first step is to form dialdehyde cellulose through periodate oxidation, and the second step is to form DALC by borohydride reduction (L. D. Verónica, Larsson, Per A. & Wågberg, 2016). The aforementioned studies were, so far, conducted on a laboratory scale; however, in recent years, efforts were made to upscale the production of the DALC fibres in batches in the tens of kilograms (Pellegrino et al. 2025).

DALC is typically produced from bleached softwood Kraft cellulose fibres, which consist of a mixture of earlywood and latewood. These fibres have cell walls composed of multiple layers, with thickness and structure influenced by growth conditions and species. Scandinavian softwood Kraft fibres generally range from 2 to 4 mm in length and 20 to 40 µm in width prior to pulping (Sjöström, 1993). Despite variability in origin, softwood fibres share a hierarchical wall structure, which includes an outer primary wall followed by three secondary layers: S1, S2, and S3. The primary wall is approximately 0.1 µm thick and contains randomly oriented nanofibrils (Aziz, 2013; Cave & Walker 1994; Sjöström, 1993). In contrast, the nanofibrils in the secondary layers are aligned at specific angles relative to the fibre axis—approximately 50–70° in S1, 5–30° in S2, and 50–90° in S3. The S1 and S3 layers are relatively thin (0.2–0.3 µm and ~ 0.1 µm, respectively), whereas the S2 layer is significantly thicker, ranging from 1 to 5 µm—thinner in earlywood and thicker in latewood. These secondary layers are arranged in a helical fashion (Aziz, 2013; Cave & Walker 1994; Sjöström, 1993), with the S2 layer contributing most significantly to the fibre's mechanical and swelling properties due to its dominant thickness.

The thermoplastic properties of cellulose-based materials are governed by a range of factors, including molecular structure, intermolecular interactions, crystallinity, fibril orientation, fibre wall architecture, chemical modifications or the presence of plasticisers (Müller et al. 2019; Nishiyama 2009; Shen & Gnanakaran 2009; Su et al. 2023; Wohlert et al. 2022). Several studies have investigated partially modified DALC fibres to understand the effect of these parameters. For instance, molecular structure has been explored by (Karlsson et al. 2024; Mehandzhiyski et al. 2022), while intermolecular interactions have been examined by (Elf et al. 2023; Kim et al. 2024). Crystallinity in DALC has been studied by (Larsson, et al. 2013; Larsson & Wågberg 2016). Structural characterisation of fibres in the dry state has been conducted using scanning electron microscopy (Larsson & Wågberg 2016). However, to the best of our knowledge, there is currently no detailed insight into the hierarchical fibre structure of DALC as a function of modification level, nor into the role of the secondary wall layers (S1, S2, and S3) in driving the morphological and structural transformations associated with chemical modification.

Existing literature on cellulose swelling with balloon-collar morphology primarily pertains to the dissolution of the cellulose-rich fibres (Burger et al. 2020; N. Le Moigne & P. Navard, 2010a; Moigne et al. 2008; Naserifar et al. 2021; Navard & Cuissinat 2006; Reza et al. 2017; Sim 2014; Singh et al. 2015; Zhang 2012). When cellulose-rich fibres are dissolved in a solvent, the dissolution undergoes a sequence of steps, including ballooning with balloon-collar morphology, the disappearance of the collar forming a highly swollen fibre, disruptions of the balloons to nanofibrils and in the latest step consisting of a solution of dissolved cellulose chains (Jardeby et al. 2005, 2004; Nicolas Le Moigne &

Patrick Navard, 2010b). However, the understanding of the morphological changes with different degrees of modification in DALC fibres, their swelling propensity at the fibre level, and the morphology of the fibre after reaching the maximum heterogeneous swelling remains unknown.

We hypothesise that the partial, regioselective modification of cellulose fibres via periodate oxidation and borohydride reduction induces morphological changes similar to those observed during the dissolution of cellulose-rich fibres. Specifically, we propose that increasing the degree of modification (DOM) leads to progressive disruption of the secondary wall layers, resulting in enhanced swelling characterised initially by balloon–collar morphologies, followed by more uniform fibre swelling at higher DOM levels. This study investigates the morphological evolution of DALC fibres across a range of DOM using optical microscopy techniques, including polarised light, differential interference contrast (DIC), and confocal laser scanning microscopy with dual fluorescent labelling. Fibre swelling propensity was further evaluated through water retention value (WRV) measurements.

Experimental

Materials

Bleached softwood Kraft fibres were sourced from Stora Enso and subsequently processed and chemically modified at RISE Processum in Örnsköldsvik, Sweden. Sodium (meta)periodate was purchased from Sisco Research Laboratories (99%), and 2-propanol from Supelco® (≥99.5%). Sodium borohydride pellets were purchased from Thermo Scientific (98%). Filter bags of analytical grade (size 2, BPENG 200 µm) were purchased from Filter Specialists Incorporated (FSI). Other chemicals, such as sodium hydroxide, isopropanol, and hydroxylamine hydrochloride, were all analytical grades.

Cellulose modification

The bleached softwood Kraft pulp was first suspended in deionised water with calcium chloride (CaCl) added to adjust the conductivity to 80 µS/cm. The fibre suspension was then subjected to beating at 160 kWh/tonne and a concentration of 3%, using a low edge load of 2.5 Ws/m to minimise the formation of fines. Following beating, water was removed, and the pulp was washed twice in a centrifuge with 80 L of deionised water per wash to eliminate residual fines. The washed and dewatered pulp was then resuspended in deionised water to a consistency of 4.5%.

Chemical modification of the fibres was carried out via oxidation with sodium periodate, followed by reduction with sodium borohydride, partially converting the cellulose into dialcohol cellulose (DALC). The reactions were performed in a 50-L stirred reactor constructed of Hastelloy (UNS N06022). A total of 39 kg of pulp suspension (4.5 wt.% consistency) was heated to 44–50 °C. Subsequently, 2.5 L of 2-propanol and 2.5 kg of sodium periodate were added. Oxidation was allowed to proceed for 45, 80, or 120 min, after which the reaction was quenched by thoroughly washing the fibre-containing filter bags with deionised water.

Following oxidation, the aldehyde content introduced into the fibres was quantified via a stoichiometric reaction with hydroxylamine hydrochloride, as described by (Zhao & Heindel 1991). This analysis yielded aldehyde contents of 3.1, 5.0, and 5.8 mmol g^{-1} of fibre, which, assuming pure cellulose, correspond to degrees of modification of 26%, 44%, and 51%, respectively. These samples are hereafter referred to as DALC26, DALC44, and DALC51.

Subsequently, a reduction step was performed to convert the aldehyde groups to primary alcohols. The oxidised fibres were resuspended in the same reactor, to which 29.5 kg of fibre suspension and 7.5 kg of ice were added. Once the temperature dropped below 4 °C, 350 g of sodium borohydride dissolved in 1.65 kg of deionised water was added over a period of three minutes. After one hour of reaction time, the fibres were thoroughly washed in filter bags with deionised water to stop the reaction and remove residual chemicals. It was assumed that all dialdehyde groups were fully reduced to dialcohol groups. The gravimetric yields of the modified fibres were 70, 40, and 30% for DALC26, DALC44, and DALC51, respectively. The solids content of the final fibre suspensions was 20% for DALC26, 15% for DALC44, and 11% for DALC51.

Assessment of molecular weight

The molecular mass (M_w) was determined by size exclusion chromatography (SEC). The dialcohol cellulose fibres were first dissolved in N-dimethylacetamide (DMAc) containing 8% lithium chloride (LiCl). This was achieved by first soaking the sample in water to swell the fibres, then four equal volume solvent exchanges into ethanol were performed, followed by four exchanges to remove water from DMAc, and finally, removal of the excess DMAc to leave behind DMAc-saturated fibres. An 8% LiCl/DMAc solution was prepared by heating DMAc at 120 °C for 60 min. Once the DMAc had cooled to about 70 °C, oven-dried LiCl was added. The solution was left overnight to ensure complete dissolution of LiCl. Once all LiCl was dissolved, the DMAc-saturated fibres were added to 8% LiCl/DMAc and left overnight under magnetic stirring to dissolve the dialcohol cellulose fibres. Finally, once the fibres were visually dissolved, the solutions were diluted for SEC analysis with LiCl-DMAc to solutions containing 1.6% LiCl. The molecular weight distributions of the DALC samples were ultimately determined by services offered by More Research (Örnsköldsvik, Sweden) using PL-GPC 220 (Santa Clara, CA, USA) with a refractive index detector with 0.5% LiCl / DMAc at a flow rate of 1 ml/min, temperature 70 °C. The columns used were 20 µm Mixed-A columns from the Polymer Lab. One guard column and two 30 cm columns in series (2016–10-14). Pullulan polysaccharide standards from Polymer Lab (2013–02-04) were used, assuming that dissolved partial dialcohol cellulose behaves like the conventional pullulan standards used for native cellulose. The molecular weight distribution of the modified fibres was determined to be 36.8, 19.1, and 20.7 for 26, 44, and 51% DOM, respectively, with corresponding polydispersity indices of 4.192, 2.375, and 2.299.

Optical microscopy and image analysis

Optical microscopy images were acquired using a ZEISS Microscope (Oberkochen, Germany) in reflected light mode using cross-polarised light mode with an exposure time of 300–330 ms and in differential interference contrast (DIC) mode, at an exposure time of 500 ms and a magnification of 100x. Imaging wet or swollen fibres required a straightforward setup using a standard glass slide (76 mm × 26 mm × 1 mm, VWR microscope slides, with cut edges frosted) and a cover slip (60 mm × 26 mm, Menzel-Gläzer, Charleston Scientific, Singapore), where the edges of the coverslip were sealed using nail polish to avoid drying before and during imaging. All the images taken were of fibres suspended in excess water. Image analysis was conducted using ImageJ software (Maryland, USA) and allowed for quantification of water-swollen cellulose fibre dimensions. 30 representative fibres for each never-dried sample were taken for accuracy. Some of the modified never-dried fibres were air-dried at room temperature for two–three days. The air-dried fibres were rewetted in excess water and gently shaken on the mixing table for four days before imaging. The DALC51 fibres were also ultrasonicated for 15 min using VWR ultrasonic cleaning bath – 50/60 Hz.

Confocal laser scanning microscopy

Confocal Laser Scanning Microscope (Leica Microsystems GmbH, Wetzlar, Germany) equipped with a 20 × water immersion objective (numerical aperture = 0.5) was used for imaging with either 1 × or 2 × electronic magnification, using the following settings: DIC = 1920 × 1200 pixels format was applied, yielding a pixel size of 0.386 µm/pixel, Confocal = 512 × 512 pixels format was applied, yielding a pixel size of 1.239 µm/pixel, and an image acquisition rate of two images per second. The pinhole size was kept at 1 Airy unit with a zoom factor of four for all experiments. A 100-mW argon laser was used, operating at a power level of 25%. Calcofluor white and fluorescein isothiocyanate (FITC) dextran with a molecular weight of 10 kDa were used for fluorescence imaging. The cellulose fibres were labelled using calcofluor. Excitation for the calcofluor was at 350 nm, and emission was collected at 432 nm. The FITC dextran, excitation was at 490 nm, and emission was collected at 520 nm. The FITC-labelled dextran was added to the sample suspension and left to defuse overnight, while calcofluor white was added right before imaging. Three representative videos for each fibre sample were taken for analysis.

Fibre analysis

A conventional Kajaani FS300 (Metso Automation, Kajaani, Finland) fibre analyser was used to assess the numerical average fibre length, according to Tappi T271(Brodin & Theliander 2013; Khosravi et al. 2022). The instrument was calibrated before use by running a sample of synthetic (rayon) calibration fibres, and fibre length determinations were achieved with the system optics adjusted to the 0–7.0 mm measuring range. Metso Automation software measured never-dried fibre samples using the Kajaani Fibre Lab from screened pulps. The Kajaani fibre analyser measures fibre length in dilute suspensions of never-dried pulps. As measurements are performed in the hydrated state, the method indirectly reflects fibre wall porosity and water accessibility through swelling behaviour, providing additional insight into fibre–water interactions.

Water retention value

Water retention value (WRV) was used to evaluate the capability of the modified cellulose sample to uptake and hold water, providing a quantitative proxy for the fibre swelling (Grignon & Scallan 1980). A UFC40SV25 Ultrafree®-CL Centrifugal Filter of pore size 5.0 µm from Sigma-Aldrich was used. A test pad of fibres with a dry mass of 0.05 g was centrifuged for 30 min. These centrifuged test pads were weighed, oven-dried at 105 °C overnight, and then weighed again, and the results were presented as g_{water}/g_{fibres} of fibres. A standard centrifugal force of 3000 ± 50 g. The test pad was used with the centrifuge, maintaining a working temperature of 23 ± 3 °C. The centrifuge was equipped with a timer and an electric brake. All the prepared modified fibre samples and the control unmodified fibre samples were measured as duplicates.

Results and discussion

Swelling of DALC fibres characterised by optical microscopy

The morphologies of the never-dried fibres were studied using DIC and polarisation mode to complement with each other in the same field of view for a better understanding of fibre morphology. Figure 1 compares fibres observed by DIC and polarisation mode imaging. The first and second columns show DIC and polarised images, respectively, from the same field of view. The top row in Fig. 1 shows unmodified, unbeaten bleached Kraft pulp fibres, exhibiting some kinks and curls (Fig. 1a, b). The DALC26 fibres display mild periodic bulging, but not full-scale ballooning, along the fibres (Fig. 1c, d). The tendency of a significant heterogeneous swelling of fibre wall is more pronounced for DALC44 fibres, in which ballooning is readily visible, with the characteristic balloon-collar-like structure (Fig. 1e, f). The DALC51 fibres appear to show the most extensive swelling and ballooning (Fig. 1g, h).

An advantage of the DIC mode is its ability to impart a pseudo-three-dimensional appearance to fibres, enhancing traditional two-dimensional microscopy images. Hence, it is possible to perceive more easily the morphological changes in the fibre, such as fibre-wall swelling, fibre damage, external fibrillation, and orientation of different regions of the fibre wall. In comparison, the polarisation mode is sensitive only to optically anisotropic fibre structures, indicating the orientation of the nanofibrils constituting the fibre wall. When delignified cellulose fibres swell heterogeneously in specific solvents, local balloon-like expansions may appear (Navard & Cuissinat 2006; Sim 2014; Sjöström, 1993). The swollen regions of DALC26 fibres retain some birefringence, observed as colourful patterns under polarized light, conceivably due to the anisotropic alignment of nanofibrils within the fibre wall. These colours arise from pitch ordering in the visible region of light, reflecting the underlying structural organization. It can be observed in unmodified and DALC26 fibres (Fig. 1a, b, c, and d) that the non-swollen regions exhibit more colour than the swollen regions. Several studies have demonstrated polarized light microscopy as a useful tool to disclose optical anisotropy, such as showing the crystalline regions through birefringent patterns in starch granules and cellulose nanocrystals (Viet et al. 2007). However, an absolute determination of Microfibril angles (MFA) using minor colour changes is not performed in this study. Birefringence arises from repeating patterns in a structure (for example, the nematic crystalline phase in cellulose nanocrystals) (Kádár et al. 2021; Richely et al. 2023). Secondly, the heterogeneously swollen

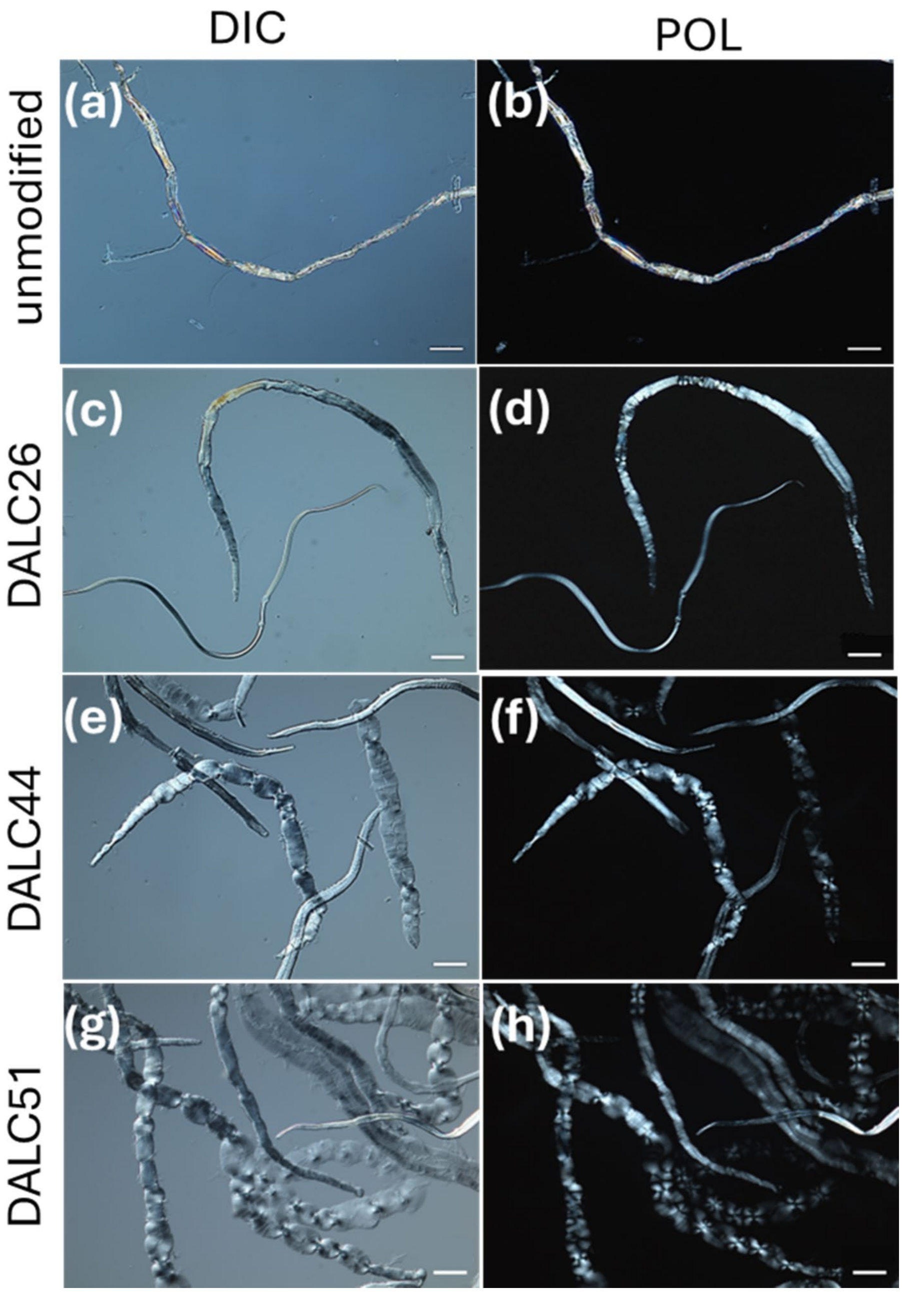

Fig. 1 Optical microscopy images in DIC mode (left column) and polarisation mode (right column). From the top row, **a**, **b** unmodified cellulose fibre; **c**, **d** DALC26; **e**, **f** DALC44; **g**, **h** DALC51. The fibres of the same DOM were imaged in the same field of view for the two modes. The scale bars correspond to 100 μm. All the images are representative of the fibre of a specific sample set

fibres (DALC44 and DALC51), can be observed showing a Maltese-cross pattern along the fibre length (Fig. 1f, and h). The Maltese-cross pattern is a specific interference pattern observed in certain birefringent materials under crossed polarizers. The appearance of the Maltese-cross in Fig. 1f and h, seen in the balloon-collar fibres demonstrates the alignment of birefringent structures interacting with polarized light, similar to observations reported by Parker et al. for cellulose nanocrystals (Parker et al. 2016). The Maltese-cross pattern and the alignment of nanofibrils in the secondary wall layers are discussed in detail in the subsequent section. Thirdly, the chemical modification has led to two modes of heterogeneous fibre swelling: (i) heterogeneous swelling among the different fibres in the same sample and (ii) heterogeneous swelling along the fibre length (causing balloon-collar structure). Such heterogeneity in swelling is presumably a result of the heterogeneity of the wood, such as late and early wood, and/or heterogeneity in the pulping process and/or post-treatment, such as beating (Sjöström, 1993). It can be observed that the fraction of fibres that contains ballons, and the fraction of ballons along the fibre length, increases with increasing DOM. The exact percentage of swollen balloons are difficult to measure but an estimate is that ~ 10, ~ 55 and ~ 70% of total fibers area visible in DIC microscope images were showing balloons in DALC26, DALC44 and DALC51, respectively. In addition, the fibres originating from early and late wood have different fibre thicknesses and MFA (Zeljko 1999), which may influence the swelling capacity of the modified DALC fibres.

A closer observation of these swollen fibres gives us an indication of the progress of balloon-collar swelling. For the DALC26 fibres, a clear mild bulging along the fibre wall was observed for a substantial population of fibres, which visibly marks the beginning of the ballooning phenomenon. The DALC51 fibres exhibit the most pronounced swelling, with a significant population of fibres displaying consistent swelling along their length (Fig. 1g and h). This aligns with a recent study on partially modified DALC fibres (55% DOM) from softwood Kraft fibres, which showed mostly homogeneous swelling with few balloon structures (Engel et al. 2025). These observations together suggest that at high degree of modification the highly swollen balloon-collared fibres transition towards a uniformly swollen state. However, both the ballon-collared and uniformly swollen fibres co-exist as demonstrated by the DALC51 (Fig. 1g and h). Additional images of different degrees of modified fibres in DIC and polarized mode are given in the supplementary information for reference (Figure S1). This type of swelling and ballooning of fibres has previously been observed when cellulose-rich fibres undergo dissolution in solvents (Naserifar, et al. 2021; Reza, et al. 2017; Zhang 2012), or are modified to high-charge contents (Sjöstedt et al. 2015).

Balloon-collar formation in DALC fibres and influence of S1 and S2 layers

Figure 2a shows two fibres marked as **1** and **2**, where **1** shows clear Maltese-cross patterns while in **2**, the Maltese-crosses are distorted. Figure 2b shows a

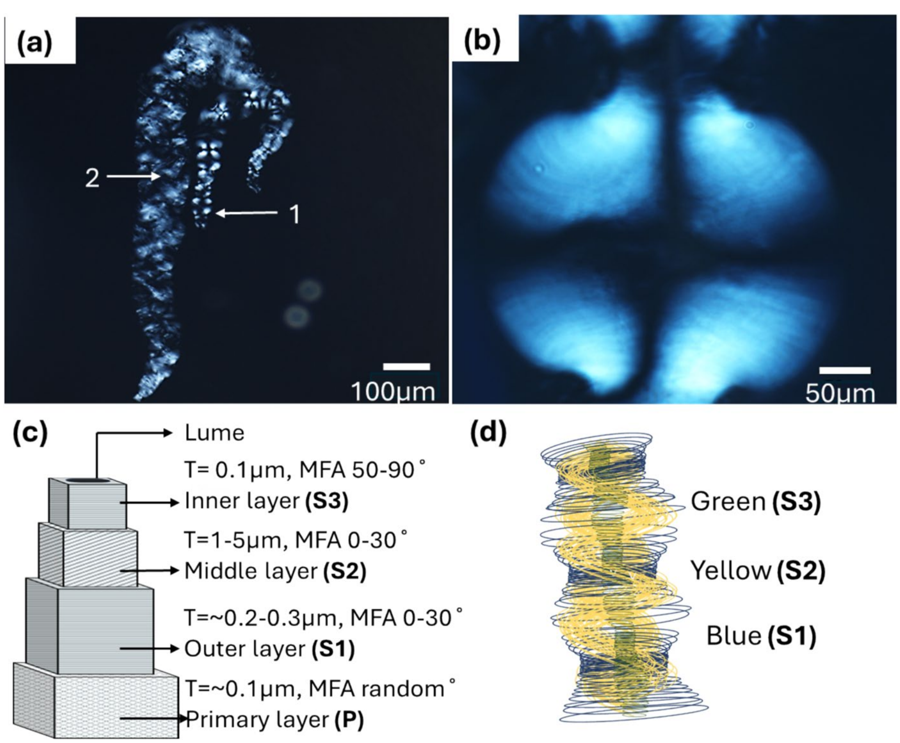

Fig. 2 **a** A uniformly swollen fibre and a heterogeneously swollen balloon in polarisation mode, **b** High-magnification optical microscopy image of a single balloon in polarisation mode, **c** A schematic illustration, not to scale, of the hierarchical structure of native cellulose fibre, **d** A schematic of the lateral-section image showing heterogeneous fibre swelling displaying balloon-collar structure

magnified image of a single balloon in polarisation mode with a Maltese-cross, which indicates the helical arrangement of the nanofibrils of the secondary wall S2 inside the balloon region. Figure 2c depicts an adapted and recreated schematic of a wood fibre wall, showing the primary wall and the three secondary wall layers (P, S1, S2, and S3) with MFA and the thickness of the secondary wall layers (Sjöström, 1993; Tabet & Aziz 2013). Figure 2d illustrates a schematic of a balloon-collared fibre, inspired by Sim et al.(Sim 2014). In this sketch, blue, yellow, and green denote the S1, S2, and S3 layers, respectively.

To better understand the results observed in Fig. 2a, we closely examined the fibre morphologies. It is evident that the Maltese-cross patterns in **1** are associated with its balloon-collar morphology, while the distorted pattern in **2** likely arises from more uniform swelling. Both fibres were also imaged in DIC mode within the same field-of-view to provide a morphological comparison (see Figure S2 in the supplementary information). Figure 2b shows a magnified image of a single balloon region under polarized light, displaying a well-defined Maltese-cross. In this optical mode, the dark arms of the cross align with the polariser and analyser axis, where light transmission is minimized, while the bright quadrants at 45° indicate regions of maximal birefringence. The images of DALC51 fibres were fractured by ultrasonication, and the cross-sectional view of a single collar region imaged in DIC and polarized mode at the same field of view for comparison are given in the supplementary information (Figure S3 and S4). This optical behaviour likely reflects anisotropic nanostructures from the microfibrillar arrangement in the S2 wall. While the Maltese-cross pattern confirms the existence of orientational anisotropy, it does not unambiguously indicate a helical arrangement of fibrils, as other structural configurations, including radial or concentric arrangements, can produce similar optical signatures. In fibres exhibiting a balloon-collar morphology, heterogeneous swelling accentuates the individual contributions of the secondary wall layers (S1, S2, and S3). Among these, the S2 layer plays a dominant role in defining mechanical response and swelling behaviour due to its relatively low MFA (typically 5–30°). This low MFA contributes to high axial stiffness and enhanced transverse deformability. As a result, the enhanced transverse deformability accommodates the swelling, which results in the formation of the balloon-collar-like structural change in response to environmental or mechanical stimuli, as previously described in the literature (Aziz, 2013; Cave 1976; Cave & Walker 1994; Sjöström, 1993).

During fibre modification, it is likely that the reagents rapidly reach the secondary wall layers of the water-swollen fibre wall. As the thickest fibre wall layer, the S2 shows the most prominent morphological changes. The emergence of the balloons can be attributed to the swelling of the S2 layer when the solvent is transported through the P and S1 walls into the thick S2 layer (Navard & Cuissinat 2006). Navard & Cuissinat also state that some regions in the S2 layer start to break into smaller fragments, heterogeneously along the fibre wall, and a fraction of the cellulose chains dissolve. During the dissolution of cellulose, small bulges along the fibre wall are created. These bulges continue to grow into balloons if there are solvents or dissolving agents in the system (Navard & Cuissinat 2006; Zhang 2012). This in turn generates an increased osmotic pressure, and to equalise the pressure differences between the surrounding and inside the fibre wall, more solvent is transported into the S2 layer (Navard & Cuissinat 2006). Ballooning depends on several factors, such as the origin of cellulose fibres, the solvent's ability to dissolve the cellulose and the mechanical properties of the fibre wall. Nevertheless, the ballooning would not have happened if the S1 layer had simultaneously been able to completely counteract the increased osmotic pressure. The S1 layer undergoes simultaneous strain due to the swelling of the S2 layer, resulting in the formation of collars. As these balloons expand, they draw substantial nanofibril bundles from the S1 layer to either side, creating the collars (Sim 2014).

Uniform swelling: the next stage of balloon-collar swelling of fibres

Figure 3a shows a DIC image of balloon-collar fibres from the previously discussed DALC51 sample. The mechanism underlying uniform fibre swelling may involve the expansion of larger balloons at the collar regions, causing these regions to swell and thereby merge adjacent balloons into a single, continuous structure. When this happens, all along the fibre length, it produces a uniformly swollen fibre. From

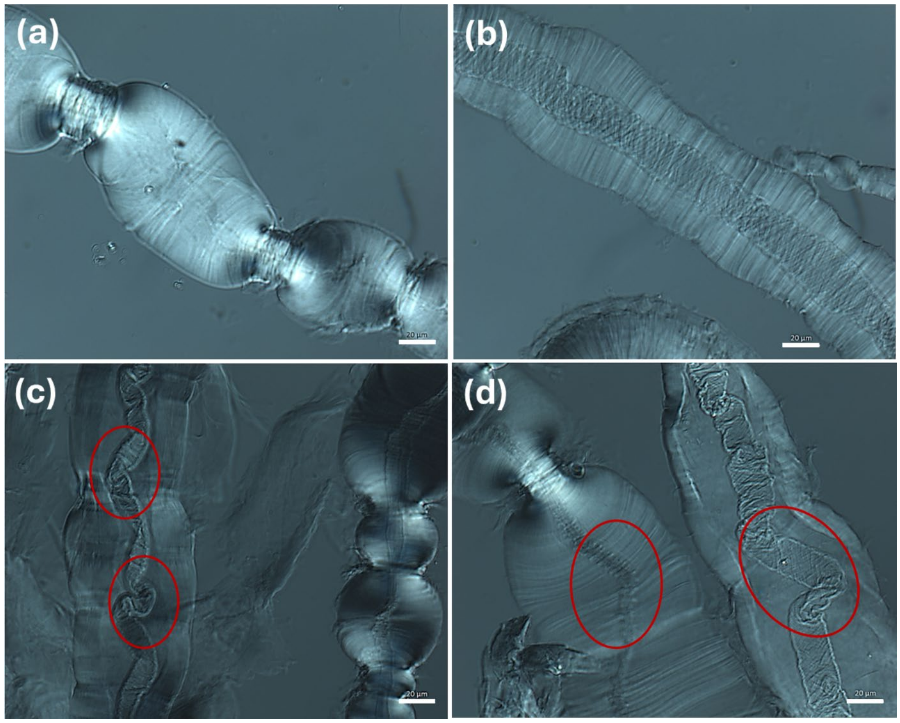

Fig. 3 **a** Heterogeneous swelling **b**, **c**, and **d** uniformly swollen DALC51 fibres in DIC mode. The fibres cut open along the fibre length show a crumbling of the S3 layer inside the swollen fibre wall, marked in red circles in (**c**) and (**d**). Scale bars correspond to 20 μm

these images, along the middle of the fibres, a helical winding is present (as indicated by the red circles in the figure). Additionally, in Fig. 3c and d, the fibres were cut open along the fibre length to view the inner layers of the fibre wall. With respect to the fibre axis, the MFA of the S1 and the S3 layers are almost similar, with ~ 50–70° and ~ 50–90°, respectively (Aziz, 2013; Sjöström, 1993). Lindström et al. have measured the MFA of Norway spruce and reported that the MFA of the S3 microfibrils is nearly 90° (Cristian Neagu et al. 2006). This indicates that the observed inner layer with helical winding may be the thinner S3 layer. Sim et al. have previously discussed this in detail with the swelling of carboxymethylated and periodate–chlorite oxidised fibres, where a similar observation of S1, S2 and S3 layers in balloon-collar fibre morphology was observed. It has also been proposed that lateral swelling of the fibres leads to a slight reduction in fibre length. According to the authors, this process subsequently induces crumpling of the S3 layer, leading to the formation of a void between the S2 and S3 layers (Sim 2014).

Despite S1 and S3 being the thinner layers, with thicknesses of 0.2–0.3 μm and approximately 0.1 μm, respectively (Sjöström, 1993; Tabet & Aziz 2013). It appears from the helical winding and its MFA that for partially modified DALC fibres, the modification does not entirely degrade the S3 layer. However, such modifications induce significant fibril swelling within each secondary wall layer, altering the morphology of the fibres. These morphological changes are influenced by both the thickness of the secondary wall layers and the MFA. In the case of the S1 layer, as previously described, the predominant S1 layer undergoes "rolling to either side" to accommodate the ballooning effect in response to the expansion of the S2 layer. Due to the similar MFA and even thinner structure compared to the S1 layer, the S3 layer is likely to experience forces from both adjacent regions (S2 layer and solvent from the lumen). Specifically, S3 layer may be subjected to an inward swelling force from the S2 layer, while simultaneously encountering an opposing force from the lumen containing the solvent. The resistance of the S3 layer to forming collars, unlike the S1 layer, may be attributed to the combined effects of two opposing forces and the helical winding of the MFA, which together create a fibrillar mesh. However, this hypothesis can only be confirmed if enough solvent is present in the lumen

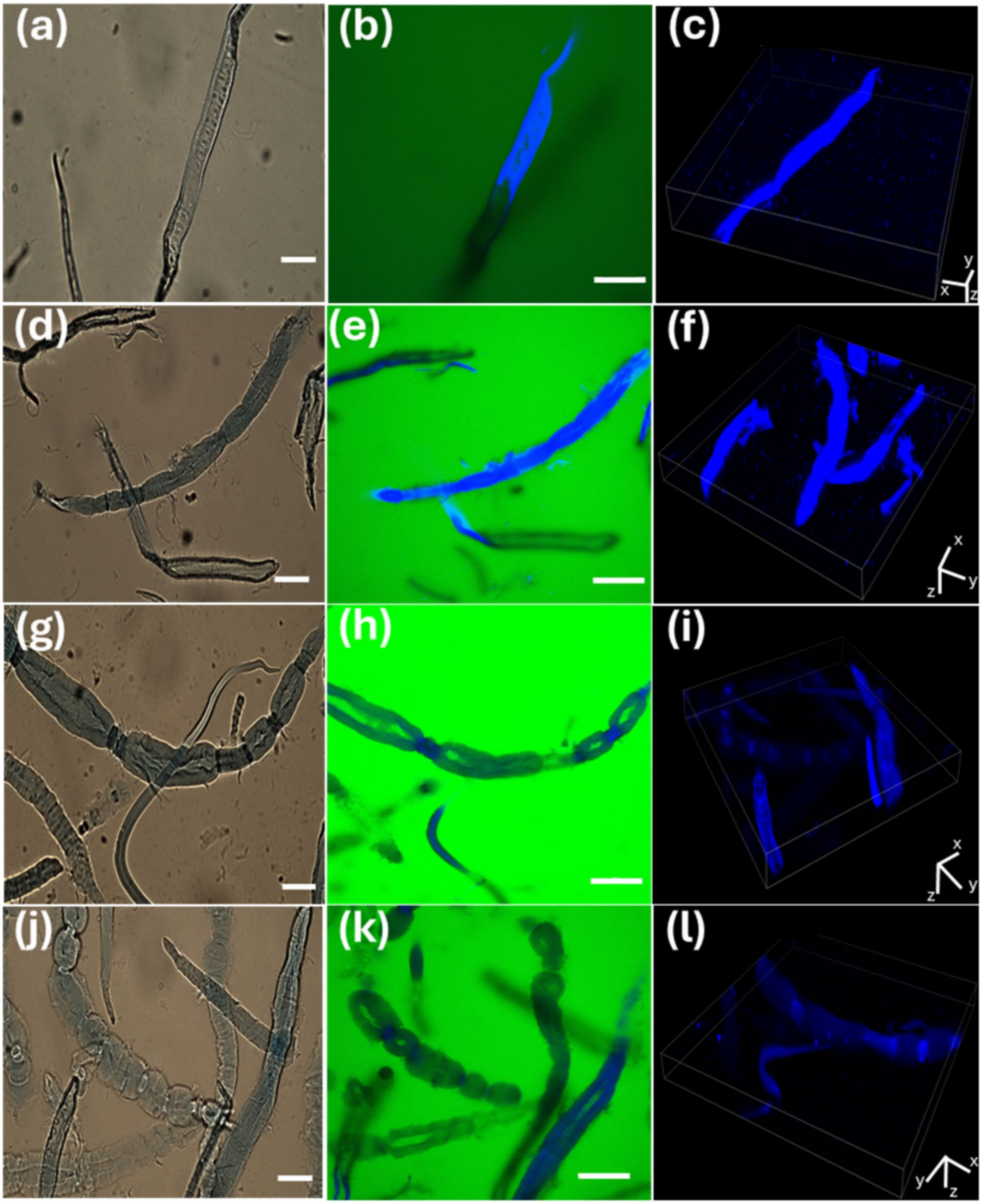

Fig. 4 LHS DIC-images of **a** unmodified, **d** DALC26, **g** DALC44 and **j** DALC51 fibres; Centre CLSM-images of dual-fluorescent labelled fibres of **b** unmodified, **e** DALC26, **h** DALC44 and **k** DALC51; Calcofluor—blue, FITC dextran—green; RHS images show CLSM of 3D z-scanned fibres of **c** unmodified, **f** DALC26, (i) DALC44, (l) DALC51. All the images in each row are in the same frame of reference for easy comparison. Scale bars correspond to 100 µm

and if the changes in lumen size with increasing fibre modification are better understood.

Using DIC and polarised images, it is difficult to clearly visualise the lumen inside the fibre wall. With an effort to understand the changes in the lumen size with increasing fibre modification, Confocal laser scanning microscopy (CLSM) with fluorescent labelling would be an ideal choice to understand these intricate details inside the swollen fibre wall.

Figure 4 shows dual-labelled fluorescent images and DIC images of swollen DALC fibres of different DOMs. For CLSM imaging of dual-fluorescently labelled fibres, FITC dextran of molecular weight 10 kDa was chosen as these molecules are assumed to penetrate the fibre wall (green). The second fluorescent label, calcofluor (blue), binds to the β-1,4 bond in polysaccharides in the fibre wall. It is evident from Figs. 4 e, h, and k that, for the higher DOM, there is an increase in the amount of water content in the centre of the fibre. Videos of z-scanned CLSM can be found in supplementary information (see videos S1-S4).

Figures 4a, d, g, and j are the DIC images of the unmodified, DALC26, – 44, and – 51 fibres, respectively. In Fig. 4b and c, the z-scanning through the unmodified fibre does not clearly show the FITC-labelled dextran inside the lumen (lack of green colour). The presence of FITC dextran in the lumen is not quite evident for the swollen unmodified fibres. However, modified fibres show a clear presence of FITC dextran in the lumen. Additionally, the FITC dextran increases with an increase in ballooning. This is evident from Figs. 4e, h, and k, where we see a gradual increase in the green colour in the middle of the fibres.

When conventional cellulose fibre networks are immersed in water, the water can be retained in the fibre network, within the lumen of fibres, and in the pores in the fibre wall. When the fibre wall expands, it swells inwards towards the lumen, reducing the size of the lumen (J.E.Stone 1968). Our experimental results, using dual-fluorescent labelling in CLSM imaging, reveal the expansion of the lumen due to ballooning of the swollen fibres. By identifying the FITC-dextran at the centre of the ballooned fibres, it is possible to indirectly show the expansion of the lumen. Presumably, the expansion of the lumen can be due to the substantial amount of nanofibril bundles from the S1 layer being pushed way to either side of the balloon to make the collar, due to which there may not be enough S1 layer left across the balloons to resist the lateral swelling. This, in turn, can lead to the inner fibre wall layers (S2 and S3) being pushed outwards, expanding the lumen. Interestingly, the above observation of lumen size expansion with increased modification of DALC fibres shows that the S3 layers resist the swelling pressure. This confirms the hypothesis of the presence of a sufficient amount of solvent in the lumen.

Swelling quantified by water retention values and fibre width measurement

Swelling propensity measured using water retention value

The WRV quantifies a fibre's ability to retain water and serves as an indirect measure of its swelling capacity. However, WRV is influenced by several factors, including fibre type, size, and mechanical properties, as well as the presence of fibre fragments, commonly referred to as fines (Forsström et al. 2005). To minimise these effects and ensure consistent measurements, fines were removed prior to WRV analysis.

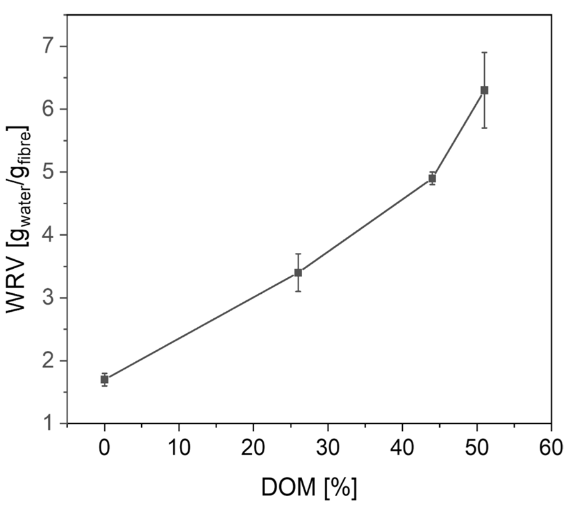

Fig. 5 WRV values assessed for unmodified and modified fibre with different degrees of modification. The WRV measurements were made on duplicates, and the error was calculated as (max–min)/2

Figure 5 shows the WRV for unmodified fibre and the different DOMs studied within this study. The unmodified fibres and DALC26 fibres had values of 1.7 g_{water}/g_{fibres} and 3.4 g_{water}/g_{fibres}, respectively. These values are similar to earlier reports (Sjöstedt, et al. 2015; Sjöstrand et al. 2019). The WRV increased further with increasing DOM. For the higher DOMs of 44 and 51%, the average WRV was 4.9 g_{water}/g_{fibres} and 6.3 g_{water}/g_{fibres}, respectively. As shown in Fig. 5, there seems to be a tendency of continuous increase with DOM for WRV. Earlier studies have also observed an increase in WRV for dialcohol cellulose (L. D. Verónica et al. 2018). This indicates an increased swelling of the fibres with increasing DOM, which could be related to an increased osmotic pressure inside the fibre wall.

Swelling propensity measured using microscopy and automated fibre analyser

To further quantify fibre swelling under water-saturated conditions, the characteristic fibre width for the different DOMs of the DALC fibres was calculated from the DIC microscopy images and measured for 30 fibres (300 points on each fibre), counting both the balloon and the collars. Figure 6a shows the distribution of the width of water-saturated fibres, determined from DIC images, while Fig. 6b shows the measured fibre width spread using Kajaani automated fibre analyser. The measured average fibre widths and the standard deviation (in bracket) from the distribution for unmodified fibres (0 DOM), DALC26, DALC44, and DALC51 were ~ 35 (9.1), ~ 40 (13.5), ~ 53 (18), and ~ 58 (24) µm, respectively. It is interesting to observe the correlation between the WRV measured and the fibre width distribution measured from DIC microscopy images, even if the techniques are completely different. The heterogeneity in swelling along the fibre length (causing balloon-collar structures), and the heterogeneity in swelling among different fibres in the same sample causes higher standard deviation. The fibre widths increased with a higher degree of modification; however, the primary effect was observed in the distribution of fibre widths rather than the individual fibre width itself. This was evidenced by a larger standard deviation, indicating greater variability in fibre dimensions with increasing modification.

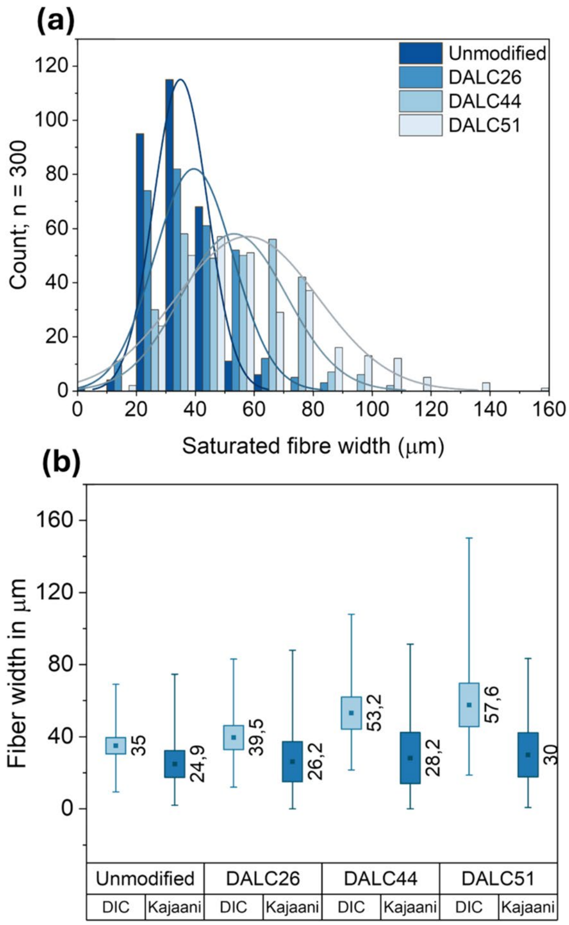

Fig. 6 **a** Fibre width distribution for DALC with different DOM and unmodified fibre, **b** Comparison of fibre width distribution measured using DIC microscopy and Kajaani automated fibre analyser

The fibre widths were also measured using a Kajaani automated fibre analyser and compared with manually measured fibre width distribution from the DIC microscopy images. The width distributions obtained were lower than those obtained through manual ImageJ analysis, and fibre widths for higher DOM showed lower values as shown in Fig. 6b. It was also observed that the cellulosic material within the balloons of the modified fibres became transparent due to the dramatic swelling of fibres and increased size of the fibre wall with deionised water, causing a decreased concentration and minimal differences in refractive indices between the inside and the outer environment of the fibres (Sim 2014). This resulted in a higher discrepancy in the measured values from

Kajaani. This discrepancy between the techniques highlights the challenges in detecting highly water-swollen and transparent modified cellulose fibres using Kajaani, which relies on polarised light to determine the fibre dimensions. As seen in Figs. 1 and 2, the birefringent patterns in the collars make it likely that the Kajaani might interpret the fibre length as the distance between two such birefringent patterns or consider it a cluster of fines. Another limitation of the Kajaani method is that the histogram of fibre widths does not extend beyond 100 µm, *i.e.* Kajaani does not perceive swollen fibres with balloon-collar morphology when widths exceeding 100 µm. Consequently, it can be concluded that the manual ImageJ analysis provided a better approach to measuring the width distribution of the modified DALC fibres due to their extensive swelling and balloon-collar morphology.

Morphological changes of the modified fibres from never-dried to air-dried and air-dried to rewetted.

Figure 7a presents a 51% DOM fibre in its never-dried state, while Fig. 7b shows the same fibre after being dried under the microscope and subsequently rewetted with deionized (DI) water, captured in the same field of view. Drying was performed under ambient conditions (relative humidity 10%, temperature 26 °C). It was observed that for the more modified fibres (such as DALC44 and DALC51), after drying,

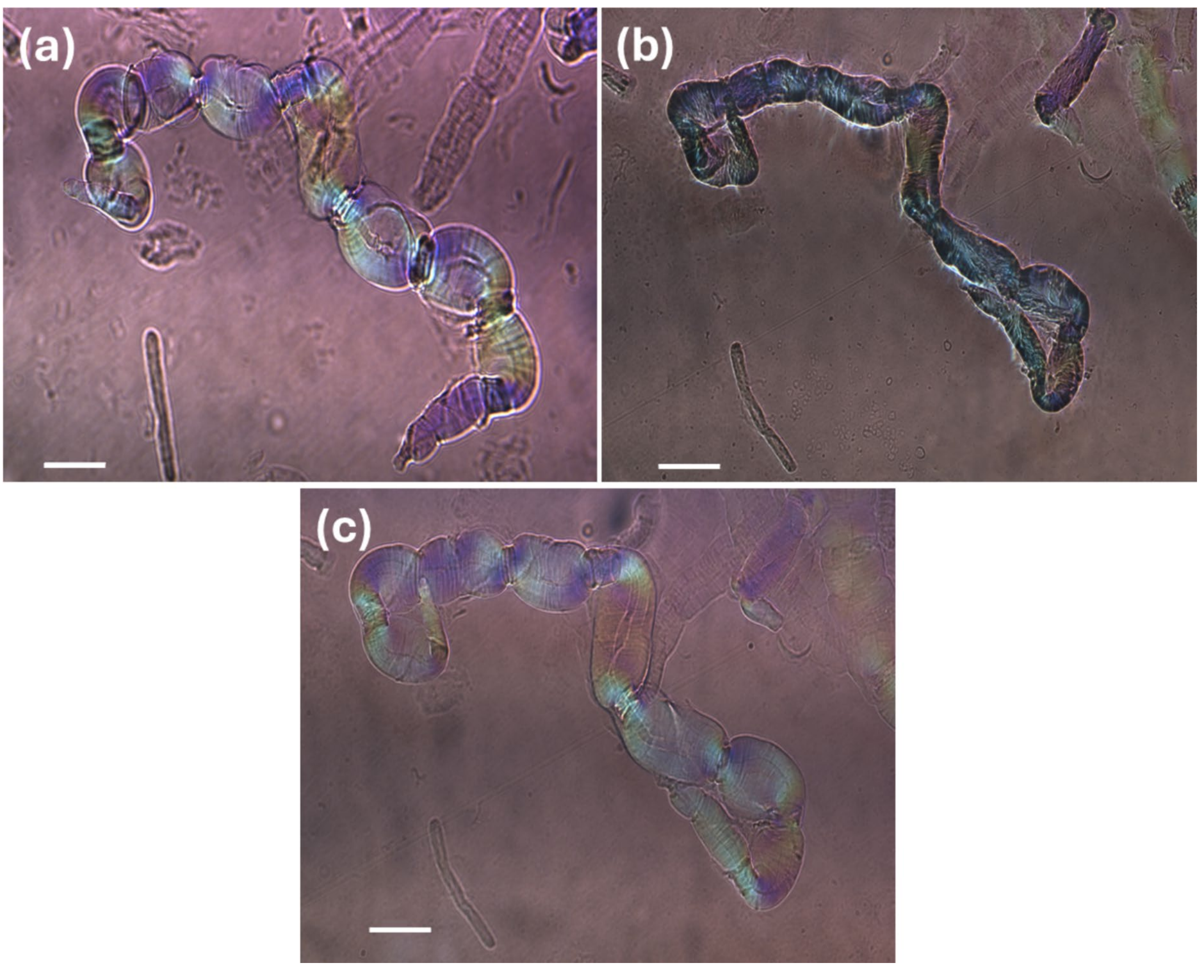

Fig. 7 DALC51 fibre in **a** never-dried, **b** air-dried, **c** rewetted conditions in the same field of view for easy comparison. Scale bar = 100 µm

the swollen fibres with balloons did not revert to the normal fibre morphology. In situ DIC microscopy video of the morphology changes in the DALC51 fibre from never-dried to dried and then rewetted conditions is given in the supplementary information (see video S5). A permanent change in fibre morphology after drying for the highly modified fibres was observed, which is in agreement with the ruptured S1 layer forming a collar. This effect is more pronounced with higher swelling and extensive ballooning, indicating an inelastic strain in the fibre wall due to modification-induced swelling. For all the samples tested, rewetting with an excess of water visually revives a fibre morphology closely resembling that of never-dried fibres. The images of the rewetted fibres for the different degrees of modification are given in the supplementary information (see Figure S5). However, the swelling propensity of unmodified Kraft fibres is known to decrease upon drying, a phenomenon referred to as hornification (Sellman et al. 2023). From Fig. 7, it is difficult to show such an effect in the rewetted fibre when compared to the never-dried fibre. This highlights the limitation of microscopy in capturing hornification in detail.

Conclusion

Morphological changes in partially modified softwood Kraft fibres (DALC26, DALC44, DALC51) were characterised using polarisation, differential interference contrast (DIC), and confocal laser scanning microscopy (CLSM) modes. The observations using micrographs show that the DALC-modified fibres experience heterogeneous lateral expansion (balloon-collar morphology) along the fibre length with the increase in the degree of modification. Microscopy observations indicate that when the fibres undergo partial heterogeneous DALC modification, it may require ~ 25% DOM to observe a mild ballooning in the swollen fibres, and ~ 50% DOM constitutes a substantial amount of uniformly swollen fibres alongside the heterogeneous balloon-collar swelling. This indicates that the heterogeneous balloon-collar swelling proceeds to a uniform swelling in DALC modified fibres. The increase in modification resulted in a greater variability in fibre dimensions, leading to a broader fibre width distribution, as indicated by a larger standard deviation. This resulted in higher discrepancies in the manually measured values by DIC image analysis from the standard techniques, like the Kajaani automated fibre analyser. For DALC fibre size analysis, our results suggest manual DIC image analysis as a more accurate technique than standard automated fibre analyser equipment.

CLSM in combination with dual fluorescent labelling gives a perspective of the condition of the lumen in the ballooned fibres and indicates that the size of the lumen appears to increase with an increase in modification. The ballooning in the never-dried fibres permanently deformed the fibre wall and hence resembled a balloon-collar morphology, even after drying. When the fibres were rewetted in deionised water, they showed a similar increase in swelling with the increase in the degree of modification. This versatile behaviour of the partially modified in dialcohol cellulose fibres, *i.e.,* large water holding capacity and large reswelling upon rewetting, is advantageous from a material use perspective as the modified fibres can be produced, dried and more efficiently transported in the dried state from one facility to another, where they can be rehydrated for further use. In addition, this dehydration–rehydration capability reduces the risk of mould growth during storage and distribution and enhances the circularity and industrial scalability of cellulose-based material systems, thereby supporting broader sustainability goals in bio-based materials development.

Acknowledgements The authors thank ProDAC, Vinnova-sponsored project within Resource Smart Processum (RSP), FibRe – Design for circularity – Lignocellulose-based thermoplastics, a VINNOVA competence centre, Department of Chemistry and Chemical Engineering, Gothenburg, Sweden.

Author contributions NV: Conceptualisation, Methodology, Validation, Formal analysis, Investigation, Resources, Data curation, Writing – original draft, Writing – review & editing, Visualisation. KJ: Materials, Resources, Supervision, and Project Administration. GLR: Project administration and financing, PL: Conceptualisation, Methodology, Formal analysis, Resources, Data curation, Writing – original draft, Writing – review & editing, Supervision, Project administration, AL: Conceptualization, Methodology, Formal analysis, Resources, Data curation, Writing – original draft, Writing – review & editing, Supervision.

Funding Open access funding provided by Chalmers University of Technology. This project Processes for DiAlcohol Cellulose PROduction – ProDAC (2021–02094) is financed by Strategiska innovationsprogrammet BioInnovation—en gemensam satsning av Vinnova, Formas och Energimyndigheten and

Tetra Pak Packaging Solutions AB and is associated with Treesearch and FibRe – Design for circularity – Lignocellulose-based thermoplastics (2019–00047), a VINNOVA competence centre.

Data availability All data and materials generated or analyzed during this study are included in this article and are available upon request.

Declarations

Conflict of interest The authors declare no competing interests.

References

Brodin FW, Theliander H (2013) A comparison of softwood and birch kraft pulp fibers as raw materials for production of TEMPO-oxidized pulp, MFC and superabsorbent foam. Cellulose 20(6):2825–2838. https://doi.org/10.1007/s10570-013-0037-x

Burger D, Winter A, Subbiahdoss G, Oberlerchner JT, Beaumont M, Tamada Y, Rosenau T (2020) Partial amorphization of cellulose through zinc chloride treatment: a facile and sustainable pathway to functional cellulose nanofibers with flame-retardant and catalytic properties. ACS Sustain Chem Eng 8(36):13576–13582. https://doi.org/10.1021/acssuschemeng.0c03492

Cave ID (1976) Modelling the structure of the softwood cell wall for computation of mechanical properties. Wood Sci Technol 10(1):19–28. https://doi.org/10.1007/BF00376381

Cave ID, Walker JCF (1994) Stiffness of wood in fast-grown plantation softwoods: the influence of microfibril angle. For Prod J 44:43–48

Cristian Neagu R, Kristofer Gamstedt E, Bardage SL, Lindström M (2006) Ultrastructural features affecting mechanical properties of wood fibres. Wood Mat Sci Eng 1(3–4):146–170. https://doi.org/10.1080/17480270701195374

Elf P, Özeren HD, Larsson PA, Larsson A, Wågberg L, Nilsson R, Chaiyupatham PT, Hedenqvist MS, Nilsson F (2023) Molecular dynamics simulations of cellulose and dialcohol cellulose under dry and moist conditions. Biomacromol 24(6):2706–2720. https://doi.org/10.1021/acs.biomac.3c00156

Engel ER, Lo Re G, Larsson PA (2025) Melt processing of chemically modified cellulosic fibres with only water as plasticiser: effects of moisture content and processing temperature. Carbohydr Polym 348:122891. https://doi.org/10.1016/j.carbpol.2024.122891

Forsström J, Andreasson B, Wågberg L (2005) Influence of pore structure and water retaining ability of fibres on the strength of papers from unbleached kraft fibres. Nord Pulp Pap Res J 20(2):176–185. https://doi.org/10.3183/npprj-2005-20-02-p176-185

Grignon J, Scallan AM (1980) Effect of pH and neutral salts upon the swelling of cellulose gels. J Appl Polym Sci 25(12):2829–2843. https://doi.org/10.1002/app.1980.070251215

Hasan I, Wang J, Tajvidi M (2021) Tuning physical, mechanical and barrier properties of cellulose nanofibril films through film drying techniques coupled with thermal compression. Cellulose 28(18):11345–11366. https://doi.org/10.1007/s10570-021-04269-9

Jardeby K, Lennholm H, Germgård U (2004) Characterisation of the undissolved residuals in CMC-solutions. Cellulose 11(2):195–202. https://doi.org/10.1023/b:cell.0000025390.81603.40

Jardeby K, GermgRd U, Kreutz B, Heinze T, Heinze U, Lennholm H (2005) The influence of fibre wall thickness on the undissolved residuals in CMC solutions. Cellulose 12(2):167–175. https://doi.org/10.1007/s10570-004-1371-9

Kádár R, Spirk S, Nypelö T (2021) Cellulose nanocrystal liquid crystal phases: progress and challenges in characterization using rheology coupled to optics, scattering, and spectroscopy. ACS Nano 15(5):7931–7945. https://doi.org/10.1021/acsnano.0c09829

Karlsson H, Svenningsson L, Storm R, Chaiyupatham P, Brolin A, Larsson A, Pinon AC, Schantz S, Karlson L, Larsson PA, Evenäs L (2024) Dynamic nuclear polarization solid-state NMR spectroscopy as a tool to rapidly determine degree of modification in dialcohol cellulose. Cellulose. https://doi.org/10.1007/s10570-024-06234-8

Khosravi H, Mehrdel P, Martínez JAL, Casals-Terré J (2022) Porous cellulose substrate study to improve the performance of diffusion-based ionic strength sensors. Membranes. https://doi.org/10.3390/membranes12111074

Kim D, Elf P, Nilsson F, Hedenqvist MS, Larsson A (2024) In-depth understanding of the effect of the distribution of substituents on the morphology and physical properties of ethylcellulose: molecular dynamics simulations insights. Biomacromol 25(7):4046–4062. https://doi.org/10.1021/acs.biomac.4c00166

Larsson PA, Wågberg L (2016) Towards natural-fibre-based thermoplastic films produced by conventional papermaking. Green Chem 18(11):3324–3333. https://doi.org/10.1039/c5gc03068d

Larsson PA, Berglund LA, Wågberg L (2013) Highly ductile fibres and sheets by core-shell structuring of the cellulose nanofibrils. Cellulose 21(1):323–333. https://doi.org/10.1007/s10570-013-0099-9

Larsson PA, Pettersson T, Wågberg L (2014) Improved barrier films of cross-linked cellulose nanofibrils: a microscopy study. Green Mater 2(4):163–168. https://doi.org/10.1680/gmat.14.00018

Le Moigne N, Navard P (2010a) Dissolution mechanisms of wood cellulose fibres in NaOH–water. Cellulose 17(1):31–45. https://doi.org/10.1007/s10570-009-9370-5

Le Moigne N, Navard P (2010b) On the Specific Behaviour of Native Cellulose Fibers upon Dissolution. Cellulose Solvents: For Analysis, Shaping and Chemical Modification, vol 1033. American Chemical Society, Washington, D.C., pp 137–148

Lo Re G, Engel ER, Björn L, Sicairos MG, Liebi M, Wahlberg J, Jonasson K, Larsson PA (2023) Melt processable cellulose fibres engineered for replacing oil-based thermoplastics. Chem Eng J 458:141372. https://doi.org/10.1016/j.cej.2023.141372

Mehandzhiyski AY, Engel E, Larsson PA, Re GL, Zozoulenko IV (2022) Microscopic insight into the structure–processing–property relationships of core-shell structured dialcohol cellulose nanoparticles. ACS Appl Bio Mater. https://doi.org/10.1021/acsabm.2c00505

Moigne N, Montes E, Pannetier C, Höfte H, Navard P (2008) Gradient in dissolution capacity of successively deposited cell wall layers in cotton fibres. Macromol Symp 262:65–71. https://doi.org/10.1002/masy.200850207

Müller K, Zollfrank C, Schmid M (2019) Natural polymers from biomass resources as feedstocks for thermoplastic materials. Macromol Mater Eng 304(5):1800760. https://doi.org/10.1002/mame.201800760

Naserifar S, Swensson B, Bernin D, Hasani M (2021) Aqueous N,N-dimethylmorpholinium hydroxide as a novel solvent for cellulose. Eur Polym J 161:110822. https://doi.org/10.1016/j.eurpolymj.2021.110822

Navard, P., & Cuissinat, C. (2006). Cellulose swelling and dissolution as a tool to study the fiber structure. *Alternative Cellulose : Manufacturing, Forming, Properties*

Nishiyama Y (2009) Structure and properties of the cellulose microfibril. J Wood Sci 55(4):241–249. https://doi.org/10.1007/s10086-009-1029-1

Parker RM, Frka-Petesic B, Guidetti G, Kamita G, Consani G, Abell C, Vignolini S (2016) Hierarchical self-assembly of cellulose nanocrystals in a confined geometry. ACS Nano 10(9):8443–8449. https://doi.org/10.1021/acsnano.6b03355

Pellegrino E, Jonasson K, Fina A, Lo Re G (2025) Plasticization of dialcohol cellulose and effect on the thermomechanical properties. Polym Degrad Stabil 235:111259. https://doi.org/10.1016/j.polymdegradstab.2025.111259

Reza M, Bertinetto C, Ruokolainen J, Vuorinen T (2017) Cellulose elementary fibrils assemble into helical bundles in S_1 layer of spruce tracheid wall. Biomacromol 18(2):374–378. https://doi.org/10.1021/acs.biomac.6b01396

Richely E, Zarei A, Melelli A, Rajan DK, Govilas J, Gabrion X, Clévy C, Legland D, Perez J, Guessasma S, Placet V, Kallio P, Beaugrand J (2023) Measurement of microfibril angle in plant fibres: comparison between X-ray diffraction, second harmonic generation and transmission ellipsometry microscopies. Compos Part c: Open Access 11:100355. https://doi.org/10.1016/j.jcomc.2023.100355

Sellman FA, Benselfelt T, Larsson PT, Wågberg L (2023) Hornification of cellulose-rich materials – a kinetically trapped state. Carbohydr Polym 318:121132. https://doi.org/10.1016/j.carbpol.2023.121132

Shen T, Gnanakaran S (2009) The stability of cellulose: a statistical perspective from a coarse-grained model of hydrogen-bond networks. Biophys J 96(8):3032–3040. https://doi.org/10.1016/j.bpj.2008.12.3953

Sim G (2014) Structure of swollen carboxylated cellulose fibers. Cellulose 21(6):4595–4606

Singh, P., Duarte, H., Alves, L., Antunes, F., Le Moigne, N., Dormanns, J., . . . Medronho, B. (2015). From Cellulose Dissolution and Regeneration to Added Value Applications — Synergism Between Molecular Understanding and Material Development: InTech.

Sjöstedt A, Wohlert J, Larsson PT, Wågberg L (2015) Structural changes during swelling of highly charged cellulose fibres. Cellulose 22(5):2943–2953. https://doi.org/10.1007/s10570-015-0701-4

Sjöstrand B, Barbier C, Ullsten H, Nilsson L (2019) Dewatering of softwood kraft pulp with additives of microfibrillated cellulose and dialcohol cellulose. BioResour 14(3):6370–6383. https://doi.org/10.15376/biores.14.3.6370-6383

Sjöström E (1993) Chapter 1 - The Structure of Wood. In: Sjöström E (ed) Wood Chemistry, 2nd edn. Academic Press, San Diego, pp 1–20

Stone JE (1968) The effect of component removal upon the porour structure of the cell wall of wood. Pulp Pap Mag Can 69(12):69–74

Su Z, Yu L, Cui L, Zhou G, Zhang X, Qiu X, Chen C, Wang X (2023) Reconstruction of cellulose intermolecular interactions from hydrogen bonds to dynamic covalent networks enables a thermo-processable cellulosic plastic with tunable strength and toughness. ACS Nano. https://doi.org/10.1021/acsnano.3c06175

Tabet, T. A., & Aziz, F. A. (2013). Cellulose microfibril angle in wood and its dynamic mechanical significance.

Tabet TA, Aziz FA (2013) Cellulose microfibril angle in wood and its dynamic mechanical significance. Cellul Fundam Asp. https://doi.org/10.5772/51105

Verma J, Petru M, Goel S (2024) Cellulose based materials to accelerate the transition towards sustainability. Ind Crop Prod 210:118078. https://doi.org/10.1016/j.indcrop.2024.118078

Verónica LD, Larsson PA, Wågberg L (2016) On the relationship between fibre composition and material properties following periodate oxidation and borohydride reduction of lignocellulosic fibres. Cellulose 23(6):3495–3510. https://doi.org/10.1007/s10570-016-1061-4

Verónica LD, Larsson PA, Wagberg L (2018) Chemical modification of cellulose-rich fibres to clarify the influence of the chemical structure on the physical and mechanical properties of cellulose fibres and thereof made sheets. Carbohydr Polym 182:1–7. https://doi.org/10.1016/j.carbpol.2017.11.006

Viet D, Beck-Candanedo S, Gray DG (2007) Dispersion of cellulose nanocrystals in polar organic solvents. Cellulose 14(2):109–113. https://doi.org/10.1007/s10570-006-9093-9

Wohlert M, Benselfelt T, Wågberg L, Furó I, Berglund LA, Wohlert J (2022) Cellulose and the role of hydrogen bonds: not in charge of everything. Cellulose 29(1):1–23. https://doi.org/10.1007/s10570-021-04325-4

Zeljko, G. (1999). Microfibril Angle in Juvenile, Adult and Compression Wood of Spruce and Silver Fir. *Phyton, Annales Rei Botanicae, Horn, 93(3)*(Plant Physiology), 129–132

Zhang S (2012) Swelling and dissolution od cellulose in NaOH aqueous solvent systems. Cellulose Chem Technol 9–10(47):671–679

Zhao H, Heindel ND (1991) Determination of degree of substitution of formyl groups in polyaldehyde dextran by the hydroxylamine hydrochloride method. Pharm Res 8(3):400–402. https://doi.org/10.1023/A:1015866104055